Journal of Theoretical, Experimental, and Applied Physics ISSN: 3070-6505

PRIME OPEN ACCESS

Volume 2, Issue 2

Research Article

Date of Submission: 04 Feb, 2026
Date of Acceptance: 13 Mar, 2026
Date of Publication: 06 Apr, 2026

The Magnetic, Magnetic Entropy and Critical Behavior Studies in La0.8Ba0.2MnO3 Around Magnetic Phase Transition Temperature

Mazhar Iqbal[1,2]*, Muhammad Nasir Khan[2], Ayaz Arif Khan[1], Khurram Shahzad[2] and Aroba Sundas[3]

[1] Department of Physics, University of Azad Jammu & Kashmir Mazaffarabad, Pakistan

[2] CDL, Physics Division, PINSTECH, Pakistan

[3] Department of Chemistry, Natinal University of Science and Technology, Pakistan

***Corresponding Author:** Mazhar Iqbal, Department of Physics, University of Azad Jammu & Kashmir Maza farabad, Pakistan; CDL, Physics Division, PINSTECH, Pakistan.

Citation: Iqbal, M., Khan, M. N., Khan, A. A., Shahzad, K., Sundas, A. (2026). The Magnetic, Magnetic Entropy and Critical Behavior Studies in La0.8Ba0.2MnO3 Around Magnetic Phase Transition Temperature. *J Theor Exp Appl Phys, 2*(2), 01-11.

Abstract

Magnetocaloric and critical phenomenon investigations were carried out in the crystalline $La_{0.8}Ba_{0.2}MnO_3$ samples prepared through solid state reaction technique. X-ray diffraction (XRD) pattern and its Rietveld refinement using Rietica software confirmed the crystalline phase purity of rhombohedral structure with space group $R\bar{3}c$. From magnetic measurements, the Ferromagnetic to paramagnetic (FM-PM) phase transition was observed at TC ~ 285K. The maximum change in magnetic entropy (ΔS_M^{max}) and relative cooling power (RCP) extracted from magnetic measurements were 3.02 J/kg K and 142.00 J/kg at an applied magnetic field $(\mu_o H)$ of 4T. Griffiths phase (GP) with a susceptibility exponent λ = 0.44 was also detected in temperature range of $T_C < T < T_G$. Critical exponential analysis indicated the 3D-Ising model like magnetic phase transition at T_C. Critical exponent's reliability was confirmed using models such as universal scaling equations of state and Widom scaling relation. Magnetic entropy change follows the law $\Delta S_M = (\mu_o H)^n$ for n = 0.46.

Keywords: Manganites, Reliability, Phase Transition, Magnetic Entropy, Magnetocaloric

Introduction

Search for the refrigeration based on magnetocaloric effect (MCE) at room temperature has gained renewed interest of researchers for the last few decades. The magnetic refrigeration (MR) has high energy efficiency with low harmful impact to the environment as compared to conventional gas refrigeration techniques. Since materials with large values of isothermal change in magnetic entropy (ΔS_M) and adiabatic change in temperature (ΔT_{ad}) are most suitable for MCE. Thus there is greater demand for the synthesis and characterization of such magnetic materials for MR in a wide temperature range with T_C in the vicinity of room temperature. The recent scientific search concentrates for the synthesis of new materials with low effective cost having high MCE over a wide temperature range in the close vicinity of room temperature. The perovskite manganites $R_{1-x}A_xMnO_3$ (R= rare earth trivalent element and A= divalent alkaline earth element) showed large MCE with different doping (x) concentrations at A site emphasizing their huge potential for application in refrigerant technology [1,2]. These doped manganites are more suitable for MR technology than Gd metal and Gd based alloys systems as they have some advantages like large resistivity, greater chemical stability and small eddy current.

The existence of ferromagnetic clusters along with paramagnetic phase above T_C results in the mixed phase known as GP. As mentioned above, the GP exist within the temperature range $T_C < T < T_G$ violating the Currie-Weiss law. The formation of ferromagnetic clusters concerned with quenched disorder and improved by the resentment between coexisting phases [3]. The mixed magnetic behavior (paramagnetic and ferromagnetic phases) of this sample for temperature range $T_C < T < T_G$ may exist due to Jahn–Teller distortion and grain-size effects [4]. The increase in the applied magnetic field reduces the ferromagnetic cluster extent in GP region and hence increased the net magnetization

[5]. The Ba doped $La_{1-x}Ba_xMnO_3$ samples possess GP and show critical behavior analogous to any of 3D-Heisenberg or 3D-Ising models [6].

The FM-PM phase transition in manganites requires the correct order of phase transition and exact universality class. The order of the magnetic phase transition around T_C is specified by the critical exponents β (which correlate the spontaneous magnetization (M_S) with temperature for $T > T_C$ at H = 0), γ (which correlate the inverse of susceptibility χ^{-1} with temperature for $T > T_C$) and δ (which correlate the critical magnetization with $\mu_o H$ at T_C) as expressed by scaling hypothesis [7].

The reported values of ΔS_M^{max} for samples $LaMnO_3$, $La_{0.9}Ba_{0.1}MnO_3$, $La_{2/3}Ba_{1/3}MnO_3$ and $La_{0.7}Ba_{0.3}MnO_3$ are 0.451

$Jkg^{-1}K^{-1}$ (at $\mu_o H$=6T), 0.665 $Jkg^{-1}K^{-1}$ (at $\mu_o H$=4T), 2.77 $Jkg^{-1}K^{-1}$ (at $\mu_o H$=1T) and 1.6 $Jkg^{-1}K^{-1}$ (at $\mu_o H$=1T) respectively. Similarly the reported values of RCP for $LaMnO_3$ and $La_{0.9}Ba_{0.1}MnO_3$ samples are 54.293J/kg and 28.83J/kg [8-12]. Already, the magnetic and magnetocaloric properties of rhombohedral $La_{0.8}Ba_{0.2}MnO_3$ sample were reported by C,-m, for low field up to 0.7T and G. Tomozlis and G. Litsardakis up to 2T but these studies were not enough for the complete description of GP and critical behavior analysis in $La_{0.8}Ba_{0.2}MnO_3$ sample for large $\mu_o H$ (~4T) [13,14]. Therefore, the complete structural, magnetic, magneto-caloric properties along with critical phenomenon studies and specific heat change up to $\mu_o H$ ~4T are required to further elaborate the magnetic refrigeration properties in this system possessing GP. The bulk $La_{0.8}Ba_{0.2}MnO_3$ material is expected to show GP and MCE as well. The MCE in this material will provide feedback for it use in MR application. The studies like the present one will help us to discover the most suitable system having large magnetic entropy and real magnetic refrigerant qualities in the vicinity of room temperature. The system is also considered as the potential candidate for magnetic sensors applications. The doping concentrations of alkaline earth atoms at R-site results in the mixed valence state of Mn (Mn^{3+} and Mn^{4+}) which transform the material from ferromagnetic/metallic to paramagnetic/insulating phase. Such transformation tuned the MCE in these materials around room temperature due to variation in doping concentration. It has been already observed that the doping concentration impact on the critical behavior and magnetic phase transition (FM-PM) temperature in manganites [15,16]. The mean field (β ≈ 0.5), the tri-critical mean field (β ≈ 0.25), the 3D-Heisenberg (β ≈ 0.365) and the 3D-Ising (β ≈ 0.325) models are employed to estimate the critical behavior and magnetic phase transition (FM-PM) in present compound.

Experimental Details

The $La_{0.8}Ba_{0.2}MnO_3$ polycrystalline sample was synthesized by solid-state reaction technique. The compounds La_2O_3, $BaCO_3$, and MnO_2 were mixed stoichiometrically in acetone. The homogeneous mixture was obtained after grinding the dry solution in an agate mortar for two hours. This dried homogeneous mixture was initially calcined at 800oC for 10 hours in a tube furnace. To get the single phase product, the calcined materials were once more grounded, palletized and sintered at 1200oC for 24 hours. Room temperature XRD spectra (XRD, Rigaku D/Max-1200X, Tokyo, Japan) verified the single-phase polycrystalline structure of $La_{0.8}Ba_{0.2}MnO_3$ sample. The refinement of the XRD pattern was performed through Rietica software which confirmed the crystalline phase purity with rhombohedral structure having $R\bar{3}c$ space group. The structural and thermal atomic parameters were also obtained from this refinement. M-T measurements were carried out at both zero field (ZFC) and 0.01T (FC), and the isothermal M-H measurements for $0 \leq \mu_o H \leq 4$ T. Isotherm measurements were carried out in the temperature range of 250-300K with a step of 3K around T_C. All magnetic measurements were carried out by using Physical Property Measurement System installed at Central Diagnostic Laboratory (CDL), PINSTECH, Islamabad. The $|\Delta S_M|$ and the MCE were determined from these MH isothermal data through Maxwell relations and were reconfirmed through different phenomenological models [17].

Results with Discussions

Structural Studies

The refined XRD pattern of $La_{0.8}Ba_{0.2}MnO_3$ sample at 300K is shown in figure 1. The sharp and distinct peaks without any impurity traces showed the rhombohedral crystalline structure with $R\bar{3}c$ space group. The Rietveld refinement using Rietica software provided the quantitative and qualitative study of crystalline structure. The refined XRD pattern displayed a good match between the measured and simulated profiles with outstanding goodness of fit χ^2 =1.94. The refined unit cell parameters are a = 5.5503 (2) Å and c =13.4770 (9)Å. In the refined XRD pattern shown in figure 1, the black dots, the red solid line and the green solid line are used to represent the experimental date, simulated data and the difference between them respectively. The blue vertical lines indicate the Bragg's peak position for $R\bar{3}c$ space group. The unit cell parameters like bond angles, bond distances and their positions obtained from refinement are listed in table 1.

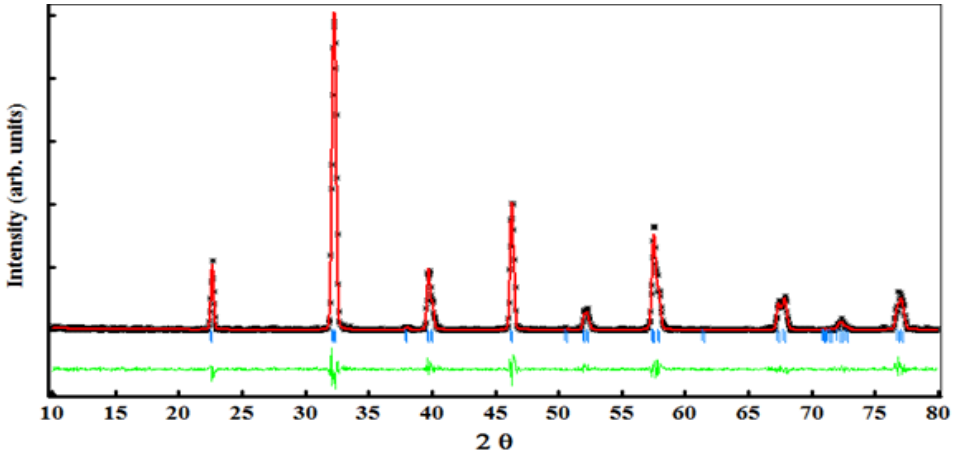

Figure 1: Refined XRD pattern of La0.8Ba0.2MnO3 Sample Measured at Room Temperature

$La_{0.8}Ba_{0.2}MnO_3$ a=5.55039(23)Å, c=13.47702(97)Å, Rp=15.29, Rwp=24.95, Rexp=17.91, GOF=1.94 and R_{BRAGG}=2.49				
	La	Ba	Mn	O
x	0	0	0	0.5411
y	0	0	0	0
z	0.25	0.25	0	0.25
B	0.64	0.64	0.41	2.95
n	0.800	0.212	1.000	3.730
La/Ba-O	3.0034(1) Å ×3	2.5470(1) Å ×3	2.7685(1) Å ×6	
O-Mn-O	90.27° ×6	89.73° ×6	180° ×3	
Mn-O-Mn	175.27°			
Mn-O	1.96993(6) Å×6			
Note: Here B is isotropic temperature factors (Å^2) and n represents the concentration of different elements in sample.				

Table 1: Structural Parameters Found from the Refinement of XRD Pattern. The Refinement Confirms the Single Phase Rhombohedral Crystalline Structure of $La_{0.8}Ba_{0.2}MnO_3$ Sample with Space Group R$\bar{3}$c

Magnetic and the Magnetocaloric Studies

The temperature dependent ZFC and FC magnetizations (MT) plots for $La_{0.8}Ba_{0.2}MnO_3$ sample are shown in figure 2a. Both MT plots showed the FM-PM magnetic phase transition at T_C. The inset of figure 2a represents the accurate value of T_C as precisely determined from the dM/dT vs. T plot. The maximum of the negative peak in dM/dT vs. T plot represents the T_C with a value of 285K. This temperature is in close vicinity of room temperature thus signifying the role of this system in the magnetic refrigeration technology. Moreover, it can be noticed that both MT plots (ZFC and FC) overlap with each other above T_C temperatures, fulfilling the criteria for paramagnetism. The bifurcation below T_C, indicates the presence of multi-domain magnetic state in the system [18].

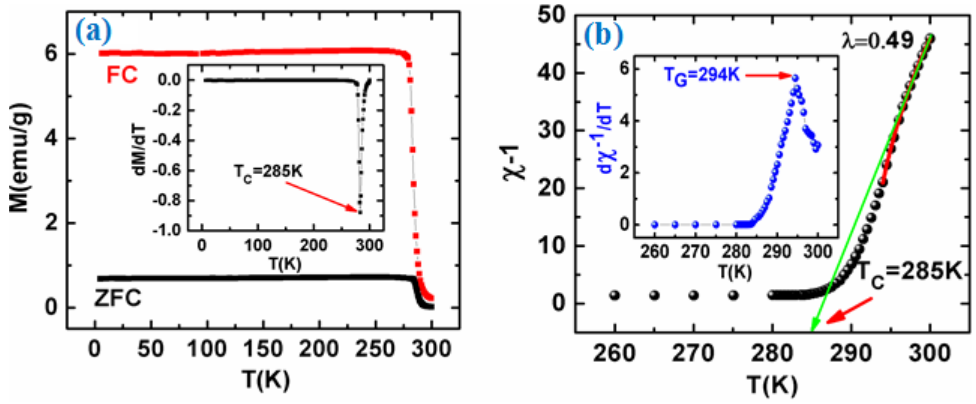

Figure 2: (a) Zero Field Cooled (ZFC) and Field Cooled (FC) M-T Patterns (For μoH= 0T and 0.01T) and (b) the χ-1 vs. T Plot Shows TC =285K along with the Plot Fitting which Gives the Value of λ=0.49. The Inset of (a) Represents the Derivative of M-T (ZFC) Pattern with Negative Peak at TC while the Inset of (b) Shows Positive Peak at TG =294K

Figure 2b represents the dc magnetic susceptibility χ^{-1} versus T plot with a curve fitting for GP. The χ^{-1} vs. T graph shows a downward trend which violates the Curie–Weiss law criterion during $T_C < T < T_G$ where T_G = 295K. The downward trend indicates the presence of the GP and can be described to the power law, $\chi^{-1} \infty (T\text{-}TC)^{(1-\lambda)}$. The value of susceptibility exponent λ should be less than unity [6]. The power law fitting with the χ^{-1} (T) data yielded λ = 0.44. The presence of GP is the sign of the existence of ferromagnetic clusters [19]. The $d\chi^{-1}$ / dT versus T plot (inset of figure 2b) showed a maximum peak at T_G.

Subsequent to the magnetic studies, we have measured the MH loops in an applied field up to ± 6T and in the temperature range from 5 ~ 300K with a step of 50K, while MH isotherms were measured in the temperature range 250 ~ 300K in a step of 3K for this system. The MH hysteresis loops indicated the pure ferromagnetic phase in the temperature range of 5 ~ 270K and then the saturation begins to shift towards the higher magnetic field with the increase in temperature, pointing the disorder in magnetic moments. This behavior is also an indication for the ΔS_M in the system. The saturation in the MH loop almost vanished for the temperature above T_C, indicating the paramagnetic behavior. Figure 3a shows the MH hysteresis loops under $\mu_o H$ up to ± 6 T in the temperature range of 5 ~ 300K with a step of 50K. All the loops possess small remanence and coercivity (inset of figure 4a). The negligible small magnetic hysteresis loss is the sign of the soft ferromagnetic nature of the system, which is also a requirement for magnetic refrigeration application [20].

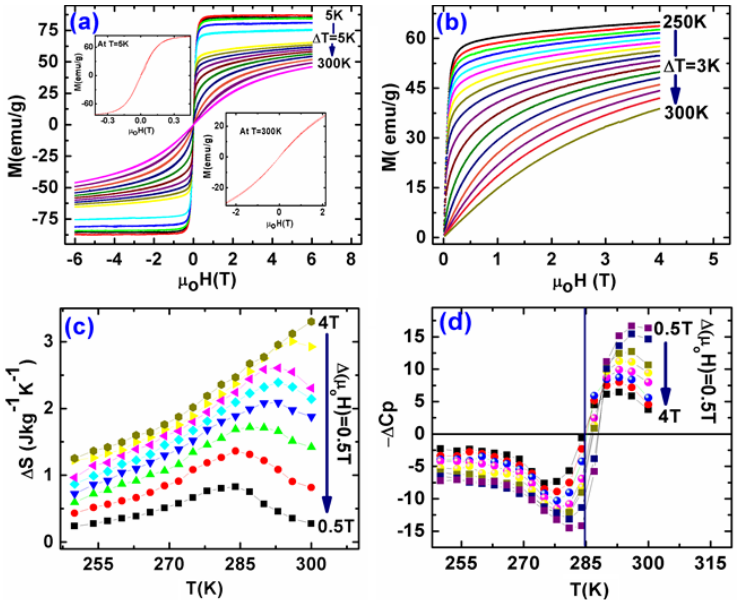

Figure 3: (a) M-H Loops for 5K ≤ T ≤ 300K with a Step of 5K (b) Shows M-H Isotherms for the Temperature Range 250-300K with the Step of 3K while (c) and (d) Shows Temperature Dependent ΔSM and ΔCp plots for different values of μoH in the vicinity of TC

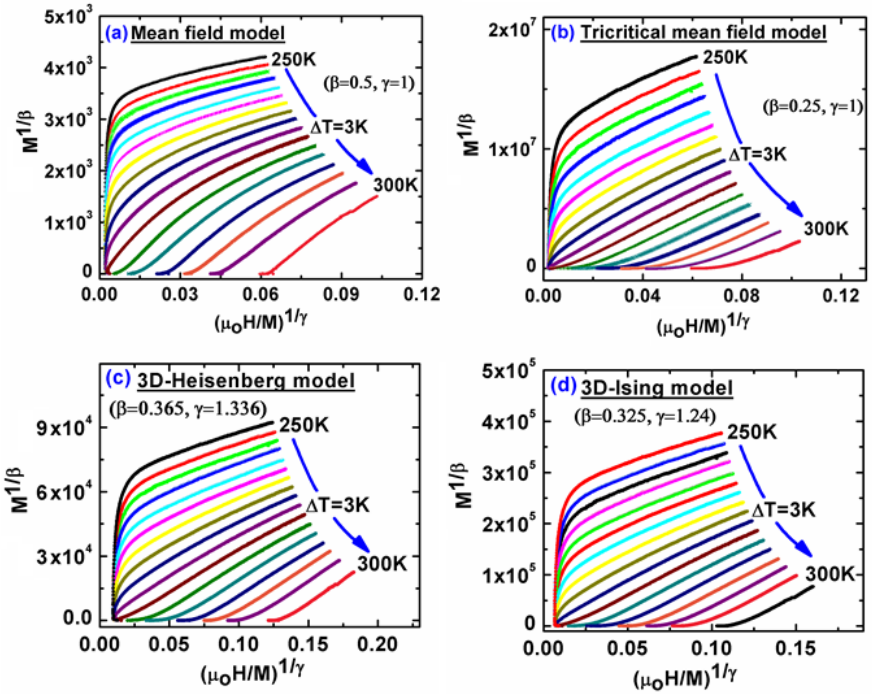

Figure 4: Represents the Modified Arrot $(\mu oH/M)^{1/\gamma}$ vs. $M^{1/\beta}$) Plots for 250K<T<300K Using Mean Field (a), Tri-Critical Mean-Field (b), 3D-Heisenberg (c) and 3D-Ising (d) Models

Figure 3b shows the MH isotherms for temperature range 250 ~ 300K in steps of 3K under varying magnetic field (H) from 0 ~ 4T. The MH isotherms showed the large increase in magnetization for low fields region and then saturated at high fields, as required for ferromagnetic material. By using the Maxwell formulas based on the thermodynamic theory, the ΔS_M (a significant thermodynamic parameter attributed to the disorder in magnetic moments) can be found from the MH isotherms, and is mathematically approximated as [17].

$$\Delta S_M(T,H) = S_M(T,H) - S_M(T,0) = \int_0^H \left(\frac{\partial S}{\partial H}\right)_T dH = \int_0^H \left(\frac{\partial M}{\partial T}\right)_H dH \quad (1)$$

For numerical data between 0 and $\mu_o H$, equation 1 can be numerically estimated as:

$$\Delta S_M\left(\frac{T_1+T_2}{2}\right) = \frac{1}{(T_2-T_1)} \int_0^{\mu_o H} [M(T_2,\mu_o H) - M(T_1,\mu_o H)] d\mu_o H \quad (2)$$

The temperature dependent magnetic entropy change (ΔS_M vs. T plots) is shown in figure 3c. It is observed that the maximum entropy change (ΔS_M^{max}) displays a peak at T_C. The ΔS_M^{max} increases with the increase in $\mu_o H$ and slightly shifts towards the higher temperature region. The maximum value of ΔS_M^{max} is 3.02J kg^{-1} K^{-1} at an applied magnetic field of 4 T. The relative variations in δT_{FWHM}, ΔS_M and RCP with respect to $\mu_o H$ are shown in table 2. [2]. The cooling efficiency of the refrigeration material can be estimated by RCP, which can be found by the relation expressed as;

$$RCP = |\Delta S_M^{max}| \times \delta T_{FWHM} \quad (3)$$

H(T)	Area($Jkg^{-1}K^{-1}$)	$\delta T_{FWHM}(K^{-1})$	$\Delta S_M(Jkg^{-1}K^{-1})$	$RCP(Jkg^{-1})$
0.5T	11.84	20.64	0.81	16.71
1.0T	21.66	26.63	1.37	36.4
1.5T	28.56	32.92	1.74	57.28
2.0T	34.72	36.12	2.10	75.85
2.5T	40.34	38.60	2.38	91.86
3.0T	48.23	41.32	2.52	104.13
3.5T	55.70	44.05	2.79	122.89
4.0T	61.42	47.01	3.02	142.00

Table 2: Relative Variations in δT_{FWHM}, ΔS_M and RCP Under Different Magnetic Fields for $La_{0.8}Ba_{0.2}MnO_3$ Sample

Here δT_{FWHM} is the full width at half maximum of ΔS_M vs. T plot representing the magnitude of heat transported between the low and high temperature regions of an ideal refrigeration reversible cycle. The found values of RCP in the $\mu_o H$ up to 4T with the step size of 0.5T are given in Table 2. From these results, it can be concluded that the system fit best for the magnetic refrigeration technology in a broader temperature range.

Critical Behavior

The Arrott plots, $M^{1/\beta}$ vs. $(H/M)^{1/\gamma}$, using mean field theory ($\beta = 0.5$ and $\gamma = 1$) explored the order of FM~PM phase transition, and are shown in Figure 4a. According to the Banerjee criterion, the positive slope of all H/M vs. M^2 plots represents the second order magnetic phase transition while the negative slope of these plots represents the first order magnetic phase transition [21]. Similarly, if the H/M vs. M^2 plot for T_C is linear and passes through the origin, and the H/M vs. M^2 plots for temperatures other than T_C are parallel to it at higher fields, then the transition is exactly according to the mean field theory [7]. From figure 4a, although the slopes are positive for all H/M vs. M^2 plots indicating the second-order magnetic phase transition but these plots not straight line and parallel to each other, hence do not fulfill the criteria of the mean field theory.

The complete study of magnetic phase transition is obtained by deeply analyzing the critical exponential phenomena. Usually, the influence of charge, lattice and orbital degree of freedom dormant in the ferromagnetic region and dominate the macroscopic magnetization. The critical parameters are determined by considering this macroscopic magnetization. In this system, the critical behavior requires an adequate model for accurate exponent's β and γ, which gives a set of parallel and linear plots. To seek such a model, we use the modified Arrott-plots ($M^{1/\beta}$ vs. $(H/M)^{1/\gamma}$) obtained from the so-called Arrott–Noakes equation of state [22].

$$\left(\frac{H}{M}\right)^{\frac{1}{\gamma}} = a\left(\frac{T-T_C}{T}\right) + bM^{\frac{1}{\beta}} \qquad 4$$

where a and b are constants.

The isothermal modified Arrott-plots (MAP), $M^{1/\beta}$ vs. $(H/M)^{1/\gamma}$, are plotted for our system in the temperature range from 250 to 300K with values of β and γ obtained from different models; the mean field model (Figure. 4a), tri-critical mean field model (Figure. 4b), 3D-Heisenberg model (Figure. 4c) and 3D-Ising model (Figure. 4d) [7,22-24].

To estimate the suitable model for our system, we have used the relative slope versus temperature (RS vs. T) plots for each model. The RS is defined as the ratio of slope of MAP at any temperature T to the slope of MAP at T_C (RS = S (T)/S (T_C)). Figure 5 represents the RS vs. T plots for each model in the vicinity of T_C. The RS value for each temperature must approach unity for a most suitable model and the MAPs for such model must have parallel lines [25]. In our case the RS values are close to unity for 3D-Ising model in the measured temperature range around Tc. Hence the obtained values of exponent's β and γ for this sample system are in accordance with the 3d-ising model.

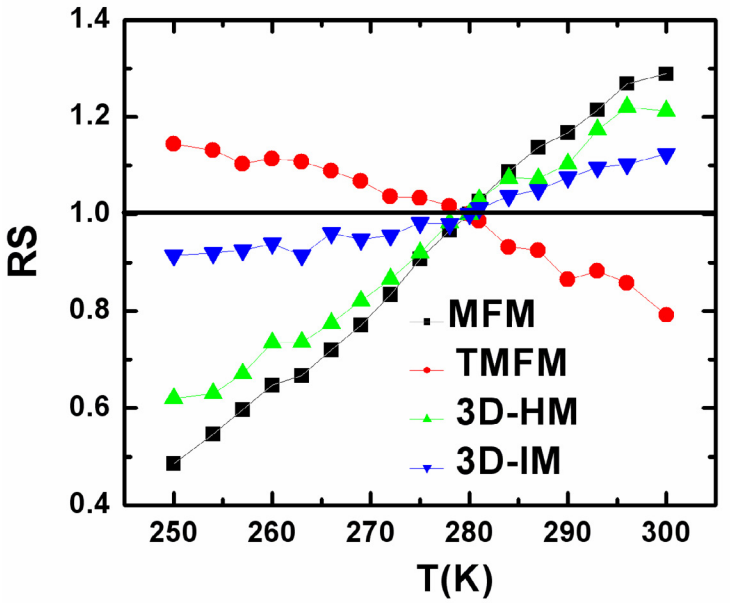

Figure 5: Represents the RS vs. T Plots for Different Models. The 3D-Ising Model Gives Almost Straight Line and is Close to RS =1

The critical exponents are defined as follows:

$$\left.\begin{aligned} M_S(T) &= M_o(-t)^{\beta}, \quad t<0 \qquad (a)\\ \chi_o^{-1}(T) &= \frac{H_0}{M_0}(t)^{\gamma}, \quad t>0 \qquad (b)\\ M &= DH^{1/\delta}, \quad t=0 \qquad (c) \end{aligned}\right\} \qquad 5$$

Where "t" is the reduced temperature $\left(t = \frac{T-T_C}{T_C}\right)$, and the constants M_o, H_o/M_o, and D are the critical amplitudes.

Following the usual practice, the data points for the spontaneous magnetization (M_S) at temperatures below T_C and the inverse susceptibility (χ_o^{-1}) at temperatures above T_C are obtained from the intercept of the linear extrapolated lines of the H/M vs. M^2 plots from the high field-region with M^2 and H/M axes, respectively (figure 4a). The spontaneous magnetization versus inverse susceptibility (M_S (T) vs. $\chi_o^{-1}(T)$) plots are shown in figure 6a. The fitting of MS (T) data with equation 5a gives the value of exponent β and the fitting of $\chi_o^{-1}(T)$ data with equation 5b gives the value of exponent γ. The obtained values of β, γ and T_C are listed in Table 3.

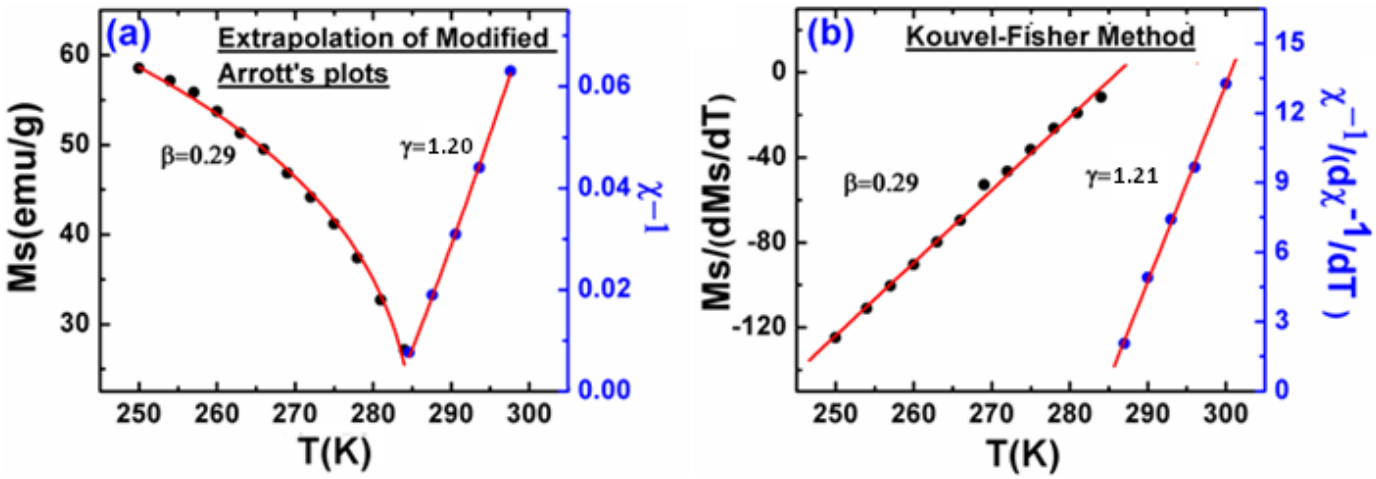

Figure 6: (a) Represents the Fitting of MS and χ-1 vs. T Plots Obtained from MAP. The Fitting of these Plots Give Values of β and γ (b) Shows the Linear Fits for Kouvel-Fisher (KF) Plots to Confirm the Values of β and γ

Moreover, the exponent's β and γ and the critical temperature T_C can also be obtained by using the Kouvel–Fisher (KF) method. The KF method provides alternative logical expressions of the power law defined as [26].

$$\left[\frac{M_S}{dM_S/dT}\right] = \frac{[T-T_C]}{\beta} \quad (6)$$

$$\left[\frac{\chi_o^{-1}}{\chi_o^{-1}/dT}\right] = \frac{[T-T_C]}{\gamma} \quad (7)$$

Using equation 6 and equation 7, $\left[\frac{M_S}{dM_S/dT}\right]$ vs. T and $\left[\frac{\chi_o^{-1}}{\chi_o^{-1}/dT}\right]$ vs. T plots (figure 6b) give straight lines. The slopes of these lines are equal to the inverse of exponent's β and γ while their intercept with temperature axes give the exact value of T_C. The obtained values of β, $_{\gamma}$, and T_C with KF method agree with those determined previously and are within limit of experimental error.

Figure 7a shows that the $M^{1/\beta}$ vs. $(H/M)^{1/\gamma}$ is linear and passes through the origin at T^C, and the $M^{1/\beta}$ vs. $(H/M)^{1/\gamma}$ plots for other temperature around T_C are parallel to it in the high field region, using experimentally found values of β and γ for this sample. Moreover, the value of δ is 4.80 obtained from the fitting of the MH plot at T_C as shown in figure 7b.

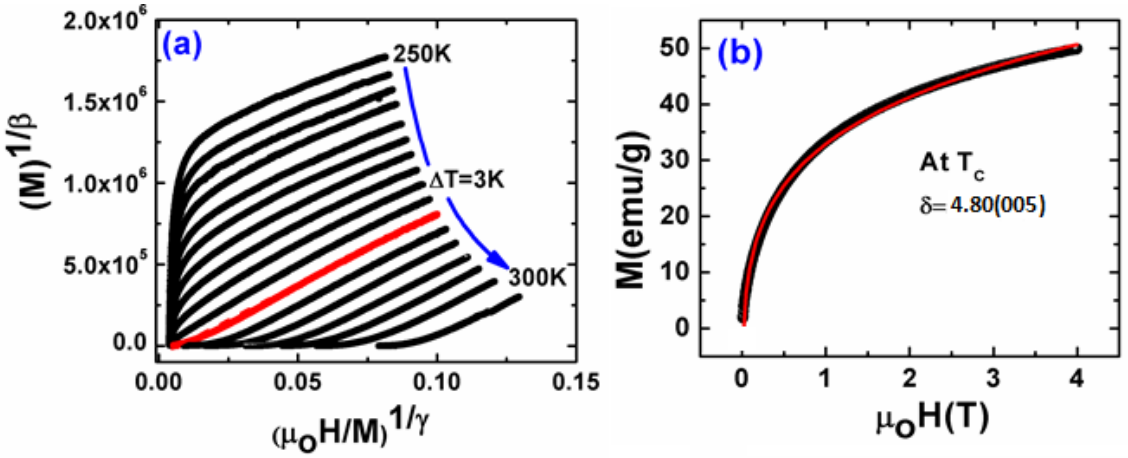

Figure 7: (a) Shows MAPs for β =0.29 and γ=1.21 Obtained and (b) Shows the Fitted M-H plot at TC which Gives the Value of Critical Exponent δ

The exponent δ was also estimated using Widom scaling relation [27].

$$\delta = 1 + \frac{\gamma}{\beta} \quad (8)$$

The obtained value of critical exponent δ~4.83 using Widom scaling relation is similar to the value obtained from the fitting of MH isotherm at T_C. It is important to note that the Widom scaling relation is the best technique to ensure the reliability of these exponents.

The scaling hypothesis is another tool to check the reliability of critical exponents which intimates that the isothermal magnetization (M) is a function of t and $\mu_o H$ in the critical region as [28].

$$M(\mu_o H, t) = t^{\beta} f_{\pm}\left(\frac{\mu_o H}{t^{\beta+\gamma}}\right) \quad 9$$

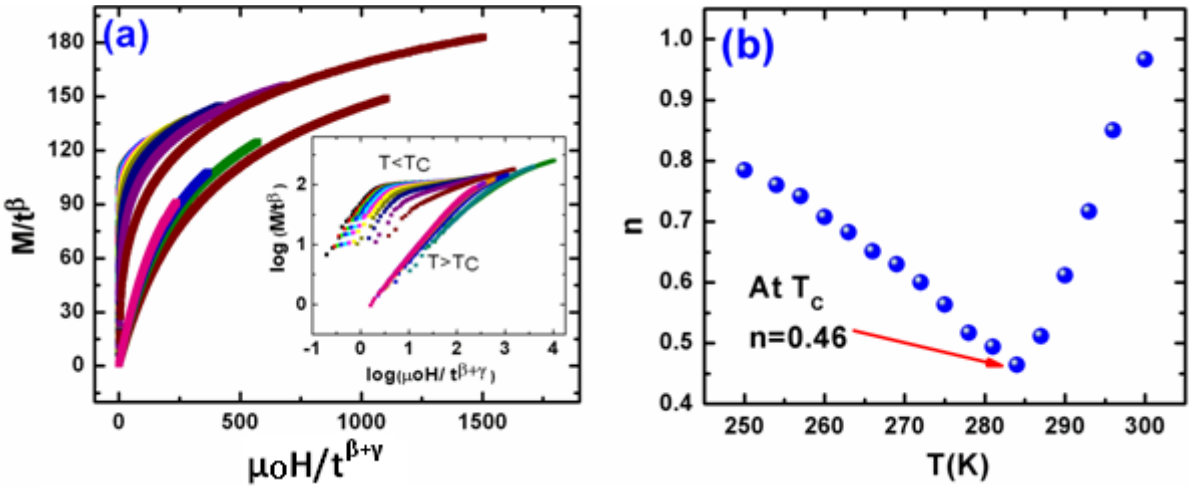

Figure 8: (a) Shows the M/t^{β} vs. $\mu oH/t^{\beta+\gamma}$ Plots Around TC and (b) Represents the n vs. T plot in Full Temperature Range. The Inset of (a) is the ln ($M/t\beta$) vs. ln ($\mu oH/t\ \beta+\gamma$) Plot at Different Temperatures Around TC fall into Two Universal Groups: One for T > TC and the Other for T < TC

Where f_+ and f_- are the analytical functions for temperatures $T > T_C$ and $T < T_C$, respectively. Using equation 9, $M(\mu_o H, t)/t^{\beta}$ vs. $\frac{\mu_o H}{t^{\beta+\gamma}}$ plots for different temperatures around T_C fall into two universal groups: one for $T > T_C$ ($t >$ 0) and the other for $T < T_C$ ($t < 0$), shown in figure 8a, confirms the authenticity of critical exponents β and γ along with T_C. The inset of figure 8a represents the data on a logarithmic scale.

SAMPLE	Technique	β	γ	δ	Curie temperature (T_C) (K)
$La_{0.8}Ba_{0.2}MnO_3$	MAP	0.29	1.20	4.82	285
	KF	0.29	1.21	4.83	285
	From fitting of M ($\mu_o H$) isotherm at T_C	-	-	4.80	-

Table 3: Experimentally Found Values of TC and Critical Exponent's β, γ and δ

The critical exponent's values along with those theoretically reported and predicted ones using different standard models are tabulated in table 3. The found values of critical exponents are listed in the table 3 which confirmed that the values of these exponents are approaches to the predicted values of 3D-Ising model. These values are slightly different from the one reported in [25]. This difference in the values of exponent's can be attributed to the different synthesis route and calcination temperature adopted, which results in the excess of oxygen concentration, hence the rhombohedral single phase structure is formed instead of orthorhombic crystalline structure [13,29-34].

The variation in the magnetic entropy change with an applied magnetic field is estimated by the power law [35].

$$\Delta S_M(H) = a(\mathrm{H})^n \quad 10$$

where power n is the function of both T and $\mu_o H$ and is used to relate the magnetic order [36]. The exponent "n" is usually obtained by the relation;

$$n = \left(\frac{d\ln \Delta S_M}{d\ln(\mu oH)}\right) \quad 11$$

The found value of n is 0.46 at T_C, which is smaller than the predicted value of n = 2/3 determined by mean field theory. This is also an evidence for our system under investigation that lies within the limit of 3D- Ising like behavior.

Moreover, at T = T_C, the power n becomes field independent and is related to the critical exponents β and γ as defined in [37].

$$n(T_C) = 1 + \frac{\beta - 1}{\beta + \gamma} \quad (12)$$

By comparing this equation with the Widom relation (δ = 1 + γ/β), we get,

$$n = 1 + \frac{1}{\delta}\left(1 - \frac{1}{\beta}\right) \quad (13)$$

From equation 13, the obtained value of n is 0.48, approaches to the value obtained from power law at T_C.

The range of exchange interaction (J(r)) is also used to estimate the universality class during PM-FM phase transition, where r stands for the range of interacting spins. From the normalization group analysis, the mathematical relation for J(r) is; $J(r) = 1/r^{d+\sigma}$, where d represents the material's dimension and σ is used for deviation of the interaction. The value of d is taken as 3 for bulk material. For three dimensional bulk material, the range of exchange interaction can be expressed as; $J(r) = 1/r^{3+\sigma}$ with $3/2 \leq \sigma \leq 2$. Usually, mean field theory valid only for $\sigma < 1/2$ with $r^{-4.5}$. Similarly, in the case of 3D-Heisenberg model, the value of σ is greater than 2 and in the 3D-Ising model and tri-critical mean field model, σ lies in the intermediate range ½ < σ <2. The correlation length exponent ν is related with γ and σ for a three-dimensional system as, ν = γ/σ. The scaling equalities α = 2 − νd, β = (2 − α − γ)/2 and δ = 1 + (γ /β) along with ν = γ/σ are used to find the value of σ [38,39]. The obtained value of σ for our system is ~1.97. Hence, the obtained value of σ lies between 0 < σ < 2, which clarify the 3D-Ising model like a transition in the system under investigation.

Conclusions

Single-phase $La_{0.8}Ba_{0.2}MnO_3$ manganite samples with rhombohedral structure were successfully prepared by solid state reaction technique. PM-FM phase transition was observed at T_C ~285K through M-T measurements. M-H isotherms for 250K ≤ T ≤ 300K explored the second-order magnetic phase transition similar to the 3D-Ising model. The ΔS_M^{max} and RCP are 3.02 J/kg K and 142.00 J/kg, respectively, at 4 Tesla. The χ^{-1} vs. T plot deviates from Curie–Weiss law for T_C < T < T_G, signifying the existence of GP with a susceptibility exponent λ = 0.44 and T_G =295K. The critical phenomenon investigated by employing models like Modified Arrott plots, Kouvel Fisher method and critical isotherms analysis. The consistency of critical exponent's was confirmed by the universal scaling equations of state and the Widom scaling relation. Similarly, the applied magnetic field dependent change in magnetic entropy (ΔS_M) verified the exponential power law $\Delta S_M = (H)^n$ with n = 0.46 at T_C.

Conflict of Interest Statement

On behalf of all authors, the corresponding author states that there is no conflict of interest.

References

1. Tishin, A. M., Spichkin, Y. I., Zverev, V. I., & Egolf, P. W. (2016). A review and new perspectives for the magnetocaloric effect: New materials and local heating and cooling inside the human body. International Journal of Refrigeration, 68, 177-186.
2. Ram, N. R., Prakash, M., Naresh, U., Kumar, N. S., Sarmash, T. S., Subbarao, T., ... & Naidu, K. C. B. (2018). Review on magnetocaloric effect and materials. Journal of Superconductivity and Novel Magnetism, 31(7), 1971-1979.
3. Debbebi, I. S., Omrani, H., Cheikhrouhou-Koubaa, W., & Cheikhrouhou, A. (2018). A-site deficiency effects on the critical behavior of La0. 6Ca0. 15• 0.05 Ba0. 2MnO3. Journal of Physics and Chemistry of Solids, 113, 67-73.
4. Rozenberg, E., Auslender, M., Shames, A. I., Felner, I., Mogilyansky, D., & Mukovskii, Y. M. (2011). 'Griffiths phase'versus chemical disorder in low-doped manganites: La0. 9Sr0. 1MnO3 crystal revisited. Journal of Applied Physics, 109(7).
5. Jiang, W., Zhou, X. Z., Williams, G., Mukovskii, Y., & Glazyrin, K. (2007). Extreme sensitivity of the Griffiths phase to magnetic field in single crystal La 0.73 Ba 0.27 Mn O 3. Physical Review B—Condensed Matter and Materials Physics, 76(9), 092404.
6. Jiang, W., Zhou, X., Williams, G., Mukovskii, Y., & Glazyrin, K. (2008). Griffiths phase and critical behavior in single-crystal La 0.7 Ba 0.3 Mn O 3: Phase diagram for La 1− x Ba x Mn O 3 (x⩽ 0.33). Physical Review B—Condensed Matter and Materials Physics, 77(6), 064424.
7. Stanley, (1971). H.E., Phase transitions and critical phenomena. Clarendon Press, Oxford.
8. Iqbal, M., Khan, M. N., & Khan, A. A. (2018). Structural, magnetic, magnetocaloric and critical behavior studies in the vicinity of the paramagnetic to ferromagnetic phase transition temperature in LaMnO3+ δ compound. Journal of Magnetism and Magnetic Materials, 465, 670-677.
9. Iqbal, M., Khan, M. N., Khan, A. A., & Zafar, N. (2018). Structural, magnetic, magnetocaloric and critical properties of La0. 9Ba0. 1MnO3 manganite. Journal of Alloys and Compounds, 769, 766-776.

10. Zhong, W., Chen, W., Au, C. T., & Du, Y. W. (2003). Dependence of the magnetocaloric effect on oxygen stoichiometry in polycrystalline La2/3Ba1/3MnO3–δ. Journal of magnetism and magnetic materials, 261(1-2), 238-243.
11. Fan, J., Ling, L., Hong, B., Zhang, L., Pi, L., & Zhang, Y. (2010). Critical properties of the perovskite manganite La 0.1 Nd 0.6 Sr 0.3 MnO 3. Physical Review B—Condensed Matter and Materials Physics, 81(14), 144426.
12. Iqbal, M., Khan, M. N., Khan, A. A., Zaka, I., Mehmood, A., & Ahmad, I. (2018). Investigation of magnetic, magnetocaloric, and critical properties of La0. 5Ba0. 5MnO3 manganite. Journal of Superconductivity and Novel Magnetism, 31(11), 3535-3544.
13. Heo, C. M., Lee, M. S., Yu, S. C., Kim, K. S., Kim, J. Y., & Lee, B. W. (2010). Magnetocaloric effect of perovskite manganites of La {sub 0.8} A {sub 0.2} MnO {sub 3}(A= Ca, Sr, Ba). Journal of the Korean Physical Society, 57.
14. Tonozlis, G., & Litsardakis, G. (2014). The structural, magnetic and magnetocaloric properties of Ba doped La manganites. physica status solidi (c), 11(5-6), 1133-1138.
15. Min, S. G., Kim, K. S., Yu, S. C., Suh, H. S., & Lee, S. W. (2005). Magnetocaloric properties of La/sub 1-x/Pb/sub x/MnO/sub 3/(x= 0.1, 0.2, 0.3) compounds. IEEE transactions on magnetics, 41(10), 2760-2762.
16. Assoudi, N., Walha, I., Nouri, K., Dhahri, E., & Bessais, L. (2018). Effect of synthesis route on structural, magnetic and magnetocaloric aspects and critical behavior of La0. 6Ca0. 3Ag0. 1MnO3. Journal of Alloys and Compounds, 753, 282-291.
17. Maxwell, J. C. (1878). Tait's "Thermodynamics".
18. Vazquez-Vazquez, C., Blanco, M. C., Lopez-Quintela, M. A., Sánchez, R. D., Rivas, J., & Oseroff, S. B. (1998). Characterization of La 0.67 Ca 0.33 MnO 3±δ particles prepared by the sol–gel route. Journal of Materials Chemistry, 8(4), 991-1000.
19. Iqbal, M., Khan, M. N., Khan, A. A., & Zafar, N. (2018). Structural, magnetic, magnetocaloric and critical properties of La0. 9Ba0. 1MnO3 manganite. Journal of Alloys and Compounds, 769, 766-776.
20. Ehsani, M. H., Kameli, P., Razavi, F. S., Ghazi, M. E., & Aslibeiki, B. (2013). Influence of Sm-doping on the structural, magnetic, and electrical properties of La0. 8− xSmxSr0. 2MnO3 (0< x< 0.45) manganites. Journal of alloys and compounds, 579, 406-414.
21. Banerjee, B. K. (1964). On a generalised approach to first and second order magnetic transitions. Physics letters, 12(1), 16-17.
22. Arrott, A., & Noakes, J. E. (1967). Approximate equation of state for nickel near its critical temperature. Physical Review Letters, 19(14), 786.
23. Stanley, H. E. (1999). Scaling, universality, and renormalization: Three pillars of modern critical phenomena. Reviews of modern physics, 71(2), S358.
24. Shin, H. S., Lee, J. E., Nam, Y. S., Ju, H. L., & Park, C. W. (2001). First-order-like magnetic transition in manganite oxide La0. 7Ca0. 3MnO3. Solid state communications, 118(7), 377-380.
25. Widom, B., Equation of state in the neighborhood of the critical point. The Journal of Chemical Physics, 1965. 43(11): p. 3898-3905.
26. Kouvel, J. S., & Fisher, M. E. (1964). Detailed magnetic behavior of nickel near its Curie point. Physical Review, 136(6A), A1626.
27. Yu, B., Sun, W., Fan, J., Lan, X., Zhang, W., Zhu, Y., ... & Yang, H. (2018). Scaling study of magnetic phase transition and critical behavior in Nd0. 55Sr0. 45Mn0. 98Ga0. 02O3 manganite. Materials Research Bulletin, 99, 393-397.
28. Xu, L., Fan, J., Sun, W., Zhu, Y., Hu, D., Liu, J., ... & Yang, H. (2017). Magnetic field-driven 3D-Heisenberg-like phase transition in single crystalline helimagnet FeGe. Applied Physics Letters, 111(5).
29. Phan, M. H., & Yu, S. C. (2007). Review of the magnetocaloric effect in manganite materials. Journal of Magnetism and Magnetic Materials, 308(2), 325-340.
30. Zhao, R., Jin, K., Xu, Z., Guo, H., Wang, L., Ge, C., ... & Yang, G. (2013). The oxygen vacancy effect on the magnetic property of the LaMnO3− δ thin films. Applied Physics Letters, 102(12).
31. Mahendiran, R., Tiwary, S. K., Raychaudhuri, A. K., Ramakrishnan, T. V., Mahesh, R., Rangavittal, N., & Rao, C. N. R. (1996). Structure, electron-transport properties, and giant magnetoresistance of hole-doped LaMnO 3 systems. Physical Review B, 53(6), 3348.
32. Kotomin, E. A., Mastrikov, Y. U. A., Gryaznov, D. V., & Shunin, Y. U. N. (2006). First principles calculations of the atomic and electronic structure of LaMnO3 (001) surface. Computer Modelling and New Technologies, 10(3), 29-40.
33. Norby, P., et al., The crystal structure of lanthanum manganate (III), LaMnO3, at room temperature and at 1273 K under N2. Journal of solid state chemistry, 1995. 119(1): p. 191-196.
34. Budhani, R. C., Roy, C., Lewis, L. H., Li, Q., & Moodenbaugh, A. R. (2000). Magnetic ordering and granularity effects in La 1− x Ba x MnO 3. Journal of Applied Physics, 87(5), 2490-2496.
35. Oesterreicher, H., & Parker, F. T. (1984). Magnetic cooling near Curie temperatures above 300 K. Journal of applied physics, 55(12), 4334-4338.
36. Dhahri, K., Dhahri, N., Dhahri, J., Taibi, K., & Hlil, E. K. (2018). Critical phenomena and estimation of the spontaneous magnetization from a mean field analysis of the magnetic entropy change in La 0.7 Ca 0.1 Pb 0.2 Mn 0.95 Al 0.025 Sn 0.025 O 3. RSC advances, 8(6), 3099-3107.
37. Fan, J., Pi, L., Zhang, L., Tong, W., Ling, L., Hong, B., ... & Zhang, Y. (2011). Investigation of critical behavior in Pr0. 55Sr0. 45MnO3 by using the field dependence of magnetic entropy change. Applied Physics Letters, 98(7).
38. Fisher, M. E., Ma, S. K., & Nickel, B. G. (1972). Critical exponents for long-range interactions. Physical Review Letters, 29(14), 917.
39. Kaul, S. N., & Basheed, G. A. (2009). Finite-size scaling in band ferromagnets with non-universal critical behavior.

Journal of Physics: Condensed Matter, 21(42), 426002.

Data Statement

X-ray diffraction (XRD) pattern of $La_{0.8}Ba_{0.2}MnO_3$ was recorded in the 2θ range of 5-90o using (DMAXB/Rigaku) diffractometer installed at Material Division PINSTECH Islamabad, in order to determine the phase purity, crystalline structure and homogeneity of the sample. XRD pattern was refined by a Rietveld refinement method using the Rietica software. The magnetization versus temperature (M-T) measurements under different applied magnetic fields (i.e. μ_oH = 0 and 0.01T) were carried out in the temperature range from 5 K to 300 K. The field dependent magnetization (M-H loops) measurements were carried out at different temperatures both above and below the critical temperature up to applied field of 6 Tesla. For MCE, M-H isotherms were measured in the temperature range from 250 K to 300 K in the steps of 3K. All magnetic measurements were done on a vibrating sample magnetometer (PPMS-Cryogenic Ltd. UK equipped with ±7 Tesla superconducting magnet) installed at CDL, Physics Division, PINSTECH, Islamabad.